

Effect of ferromagnetic film thickness on magnetoresistance of thin-film superconductor-ferromagnet hybrids

A.Yu. Aladyshkin,^{1,2,*} A.P. Volodin,³ and V.V. Moshchalkov¹

¹*INPAC – Institute for Nanoscale Physics and Chemistry, Nanoscale Superconductivity and Magnetism and Pulsed Fields Group, K.U. Leuven, Celestijnenlaan 200D, B-3001 Leuven, Belgium*

²*Institute for Physics of Microstructures, Russian Academy of Sciences, 603950 Nizhny Novgorod, GSP-105, Russia*

³*INPAC – Institute for Nanoscale Physics and Chemistry, Scanning Probe Microscopy Group, K.U. Leuven, Celestijnenlaan 200D, B-3001 Leuven, Belgium*

(Dated: May 10, 2010)

We study the influence of the thickness D_f of the plain ferromagnetic (F) film on the electrical resistance of the flux-coupled hybrids, consisting of superconducting (S) Al film and multilayer [Co/Pt] F film with out-of-plane magnetization. The behavior of such hybrids at high and low temperatures is found to be different: the nucleation of superconductivity at high temperatures is governed mainly by the typical lateral dimensions of the magnetic domains, while low temperature properties are determined by topology of the magnetic template. We show that an increase in the D_f value leads to a broadening of the field- and temperature intervals where non-monotonous dependence of the superconducting critical temperature T_c on the applied magnetic field H is observed (for demagnetized F films). Further increase in the D_f value results in a global suppression of superconductivity. Thus, we determined an optimal thickness, when the non-monotonous dependence $T_c(H)$ can be observed in rather broad T and H range, what can be interesting for further studies of the localized superconductivity in planar Al-based S/F hybrids and for development of the devices which can exploit the localized superconductivity.

PACS numbers: 74.25.F- 74.25.Dw 74.78.Fk 74.78.Na

I. INTRODUCTION

Recent technological achievements make it possible to fabricate hybrid structures superconductor-ferromagnet (S/F) in which the magnetic field produced by ferromagnetic elements varies in space at submicron scales¹ comparable with the magnetic field penetration depth λ , the effective penetration depth λ^2/D_s or the superconducting coherence length ξ (D_s is the thickness of superconducting film). In the magnetically coupled S/F hybrids the interaction between the superconducting and ferromagnetic subsystems occurs mainly via slowly decaying stray field. It is natural to expect that the magnetic field induced by the ferromagnet will strongly affect the thermodynamical, magnetic and transport properties of the considered hybrid systems (for review see Refs.¹⁻⁴ and references therein). The properties of the ferromagnetic superconductors and the S/F hybrids with rather strong exchange interaction between superconductor and ferromagnet were discussed in the reviews⁵⁻⁸. Hereafter we will focus only on the flux-coupled S/F hybrids.

It is already well known⁹⁻¹⁹ that the nonuniform magnetic field can modify the conditions for the appearance of superconductivity due to the effect of a local field compensation. This leads to an exotic non-monotonous dependence of the superconducting critical temperature T_c on an external magnetic field H applied perpendicular to the superconducting film. Depending on the topology of the magnetic field, nucleation of superconductivity in the compensated regions (near the $|B_z|$ minima, B_z is the perpendicular component of the total magnetic field) results in either the field-induced superconductivity,

or the domain-wall superconductivity (DWS) and the reverse-domain superconductivity (RDS). The field-induced superconductivity is inherent for the S/F hybrids with the arrays of ferromagnetic dots,¹⁴⁻¹⁷ whereas DWS and RDS are typical for the planar S/F hybrids with domain structure in ferromagnetic layer.¹⁶⁻²³ The problem of the formation of the localized superconductivity in the presence of one-dimensional domain structure with out-of-plane magnetization was considered theoretically in Refs.¹¹⁻¹³ It was demonstrated that superconductivity localized near the magnetic domain walls (DWS) at $H = 0$ can be realized under certain restrictions on the main parameters of the S/F hybrid,¹³ namely: (i) the magnetization M_0 of the ferromagnet, (ii) the width of the domains L , as well as (iii) the thicknesses of the superconducting and ferromagnetic films D_s and D_f . On the contrary, the RDS regime in which superconductivity appears above the magnetic domains of the opposite polarity with respect to the H sign, is considerably less sensitive to these parameters. The RDS regime is always realized for rather large $|H|$ values.⁴ The influence of the non-uniform magnetic field of the magnetic domains on the transport properties of the thin superconducting films was recently studied for the following planar low- T_c S/F hybrid structures: Nb/BaFe₁₂O₁₉ (Refs.^{19,20}), Pb/BaFe₁₂O₁₉ (Ref.²¹), Nb/PbFe₁₂O₁₉ (Ref.²²), Al/BaFe₁₂O₁₉ (Refs.²³⁻²⁵), Al/[Co/Pt]_n (Refs.^{16,17}), Nb/[Co/Pt]_n (Refs.^{18,26}), NbN/[Co/Pt]_n (Refs.^{27,28}), MoGe/GdNi (Ref.²⁹), Pb/FeNi (Ref.³⁰), NbSe₂/FeNi (Ref.³¹), MoGe/FeNi (Refs.^{32,33}).

The main focus of the paper is to investigate experi-

mentally the influence of the thickness D_f of the ferromagnetic film on the electrical resistance of the thin-film planar S/F hybrids, composed of superconducting Al film and multilayered $[\text{Co}/\text{Pt}]_n$ ferromagnetic film. Similar $[\text{Co}/\text{Pt}]$ -based hybrid structures, characterized by out-of-plane magnetic anisotropy, were recently used for the studying of the influence of the inhomogeneous field and the width of the domains on the shape of the phase transition line $T_c(H)$.^{16–18} However now we study the variation of the resistance not only at temperatures close to the superconducting critical temperature T_c , but also at low temperatures when the superconducting order parameter is well developed.

We expect that the thickness of ferromagnet as well as the typical width of the magnetic domain is also of importance for the reentrant superconductivity. Indeed, the spatial distribution of the magnetic field induced by the domain structure depends substantially on the ratio between D_f and L : the magnetic field is almost uniform inside the domains at $L \ll D_f$ and it is highly inhomogeneous in the opposite limit.¹³ Thus, one can anticipate that the thicker ferromagnetic films will have a stronger influence of the superconducting properties of the S/F hybrid. The advantage of the use of the ferromagnetic $[\text{Co}/\text{Pt}]_n$ multilayers is that we can precisely control the thickness by choosing the number n of the bilayers in the preparation process. We use thin aluminum films as a superconducting material since aluminum has the maximal coherence length (or the minimal upper critical field) among other superconducting materials.¹⁶ Therefore thin Al films should be very sensitive to the parameters of the built-in magnetic field in the S/F hybrid.

We expect that the presented comparative study might be useful for further investigations of the domain-wall superconductivity in the S/F hybrids by means of local probe techniques (e.g., scanning tunnelling microscopy/spectroscopy). Since at low temperatures the scan range of the scanning tunnelling microscope (STM) is of the order of μm , it is necessary to find the S/F system with persistent small-scale domain structure and rather high amplitude of the magnetic field. Ferromagnetic single crystals $\text{BaFe}_{12}\text{O}_{19}$ and $\text{PbFe}_{12}\text{O}_{19}$ can be hardly used for this purpose since the magnetic domains are rather large (from 2 to 30 μm) and they are strongly influenced by the external magnetic field.^{19,22} On the other hand, parallel magnetic domains in permalloy (FeNi) films have sub-micron width, however they generate too weak stray field in order to induce the localized superconductivity at low temperatures.^{32,33} In this sense the multilayered $[\text{Co}/\text{Pt}]$ structures seem to be the most suitable for the direct visualization of the DWS and the only question is what are the optimal composition of such class of the S/F hybrids. Finally, we believe that our study might be useful for development of the superconducting electronic devices based on planar S/F hybrid structures which can exploit the effect of the localized superconductivity.

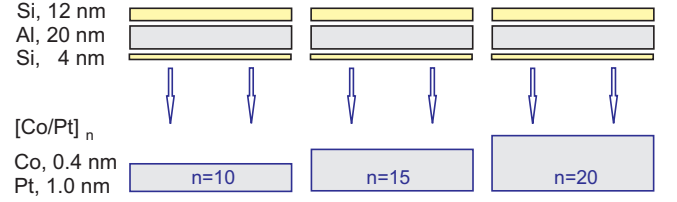


FIG. 1: (color online) Schematic presentation of the planar S/F hybrids under investigation.

II. MAGNETIC PROPERTIES OF FERROMAGNETIC SUBSTRATES

Sample preparation. In order to investigate the effects of nonuniform magnetic field, induced by bubble magnetic domains, on the magnetoresistance of thin superconducting Al films, three planar hybrid samples were fabricated by means of molecular beam epitaxy on SiO_2 substrates. The ferromagnetic part of the S/F hybrids consists of a Pt(2.5 nm) buffer layer covered by a multilayer of $[\text{Co}(0.4 \text{ nm})/\text{Pt}(1.0 \text{ nm})]_n$, where the number of the bilayers n was equal to 10, 15 and 20. All these templates were covered with a 4 nm thick Si layer followed by a superconducting Al layer of 20 nm thickness. Finally, the capping Si layer (12 nm) was evaporated in order to prevent oxidation and mechanical damage of the samples. It is important to notice that all insulating/superconducting materials were evaporated simultaneously in a single run, therefore the only difference in the sample's composition is the thickness D_f of the ferromagnetic films: $D_f = 16.5 \text{ nm}$ ($n = 10$), $D_f = 23.5 \text{ nm}$ ($n = 15$), and $D_f = 30.5 \text{ nm}$ ($n = 20$). For brevity, we introduced notations n-10, n-15 and n-20 in order to refer to the hybrid samples containing the ferromagnetic films with 10, 15 and 20 bilayers, correspondingly. Since the Al films were electrically insulated from the ferromagnetic substrate, we expect that the interaction between ferromagnetic and superconducting parts in our samples is purely magnetostatic in origin and the proximity effect is negligible.

Magnetization loops M vs. H . The hysteresis $M(H)$ loops of the ferromagnetic multilayered Co/Pt films of the different thickness were measured using a commercial SQUID magnetometer in a perpendicular applied field H at $T = 300 \text{ K}$ and $T = 5 \text{ K}$ (above the critical temperature of superconducting transition $T_{c0} = 1.45 \text{ K}$), see Fig. 2. Such ferromagnetic structures are known to possess well-defined out-of-plane magnetization.³⁴ We demonstrated that the increase in the thickness of the ferromagnetic film apparently leads to a lowering of the coercive fields: $H_{c,10}^{5K} = 4.66 \text{ kOe}$ (n-10), $H_{c,15}^{5K} = 4.02 \text{ kOe}$ (n-15), and $H_{c,20}^{5K} = 3.56 \text{ kOe}$ (n-20). We would like to note that the saturated magnetization M_s (the total magnetic moment divided by the volume) at low temperatures is practically independent on the thickness of the ferromagnetic film: $M_{s,10}^{5K} = 570 \text{ emu/cm}^3$, $M_{s,10}^{5K} =$

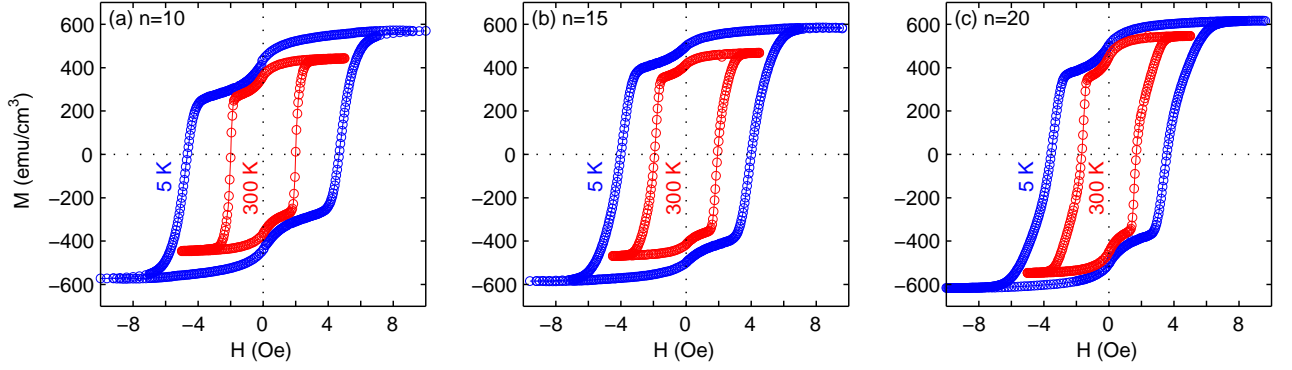


FIG. 2: (color online) Magnetization curves $M(H)$ for the ferromagnetic substrates consisting of Pt(2.5 nm) layer covered by a multilayer of $[\text{Co}(0.4 \text{ nm})/\text{Pt}(1.0 \text{ nm})]_n$, where the number of the bilayers are equal to (a) $n = 10$, (b) $n = 15$, and (c) $n = 20$. The inner $M(H)$ loops marked by red circles were measured at room temperature, while the outer loops (blue circles) correspond to $T = 5 \text{ K}$.

580 emu/cm³, $M_{s,10}^{5K} = 610 \text{ emu/cm}^3$. It is easy to see that the increase in temperature substantially reduces the width of the hysteresis loops (the corresponding coercive fields at $T = 300 \text{ K}$ are equal to $H_{c,10}^{300K} = 1.99 \text{ kOe}$, $H_{c,15}^{300K} = 1.93 \text{ kOe}$ and $H_{c,20}^{5K} = 1.68 \text{ kOe}$) and decreases the saturated magnetization M_s .

Following to the idea proposed in Refs.^{16,17,35}, we can obtain any desirable remanent magnetization M_{rem} of the ferromagnet using the following procedure of incomplete demagnetization: $H = 0 \Rightarrow 10 \text{ kOe} \Rightarrow H_{ret} \Rightarrow 0$ (Fig. 3), where H_{ret} is the so-called returning value, $H_{ret} < 0$. The dependence M_{rem} vs. H_{ret} at $T = 300 \text{ K}$ and $T = 5 \text{ K}$ for all samples are shown in Fig. 4. Al-

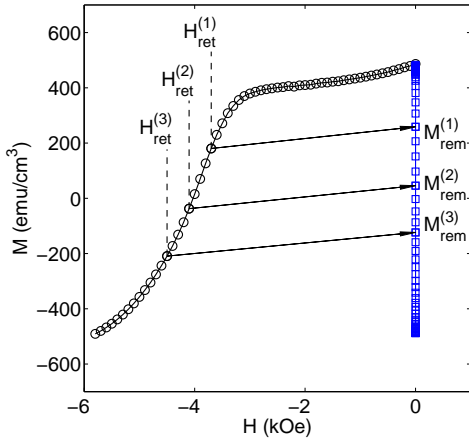


FIG. 3: (color online) Presentation of a method of preparation of the magnetic state with desirable remanent magnetization for a positively magnetized ferromagnetic film. The left curve (black circles) shows the descending branch of the typical $M(H)$ dependence measured for the sample $n=15$ at $T = 5 \text{ K}$. Depending on the returning field $H_{ret} < 0$, one can get the remanent magnetization M_{ret} at will (blue squares).

though the magnetic patterns, obtained by this procedure, appear to be metastable, the prepared magnetic states are rather robust. At least, as we can conclude from the reproducibility of experimental data, they have not been substantially changed by the magnetic field applied during the transport measurements (Section III).

MFM study of magnetic patterns. An almost perfect coincidence of the normalized hysteresis loops $M(H/H_c)/M_s$ for $T = 300 \text{ K}$ and $T = 5 \text{ K}$ indicates that the magnetization reversal processes at low and room temperatures are expected to be quite similar. Therefore magnetic force microscopy (MFM) performed at room temperature can provide an additional valuable information concerning a reshaping of the bubble magnetic domains in the ferromagnetic films at low temperatures, occurring during the process of the incomplete demagnetization.

The magnetic domain structure corresponding to the different remanent states in the Co/Pt multilayers was investigated by MFM technique at room temperature in the presence of the external magnetic field similar to that reported in Ref.¹⁹ The MFM measurements were carried out using a commercial Autoprobe M5 (Veeco Instruments) scanning probe microscope. The MFM tip was maintained at a fixed “flying” height (10–20 nm) above the sample in order to exclude the tip influence effects which can modify the magnetic domain structure. The tip oscillation amplitude was about 20 nm. With indicated scan heights in the flying mode this equates to an average tip-to-sample distances of 30–40 nm. The standard non-contact mode of scanning probe microscopy with ac cantilever amplitude stabilization was used. The dc deflection response of the MFM cantilever was used to plot the magnetic interactions between the tip and sample as a function of the tip position. The magnetic force interaction is related to the vertical component of the spatial derivative of the magnetic field from the sample. Therefore, MFM is sensitive to the strength and po-

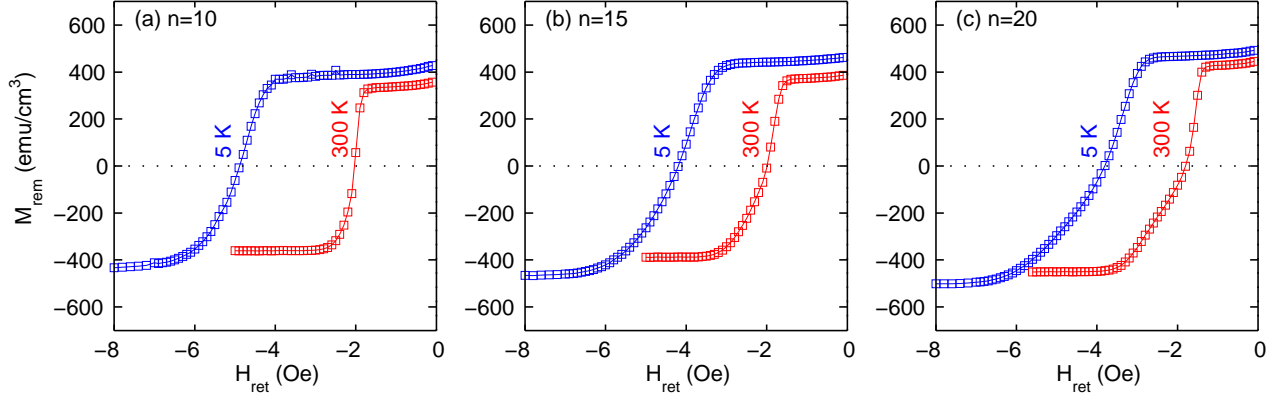


FIG. 4: (color online) Dependence of the remanent magnetization M_{rem} of the ferromagnetic film $[\text{Co}(0.4 \text{ nm})/\text{Pt}(1.0 \text{ nm})]_n$ on the returning field H_{ret} measured at $T = 300 \text{ K}$ and $T = 5$: (a) sample $n=10$, (b) $n=15$, and (c) $n=20$. Note that all these curves $M_{rem}(H_{ret})$ are similar to the descending branches of the $M(H)$ loops but not identical to that since the remanent magnetization was always measured at $H = 0$. The arrows mark the corresponding coercive fields H_c , where $M = 0$.

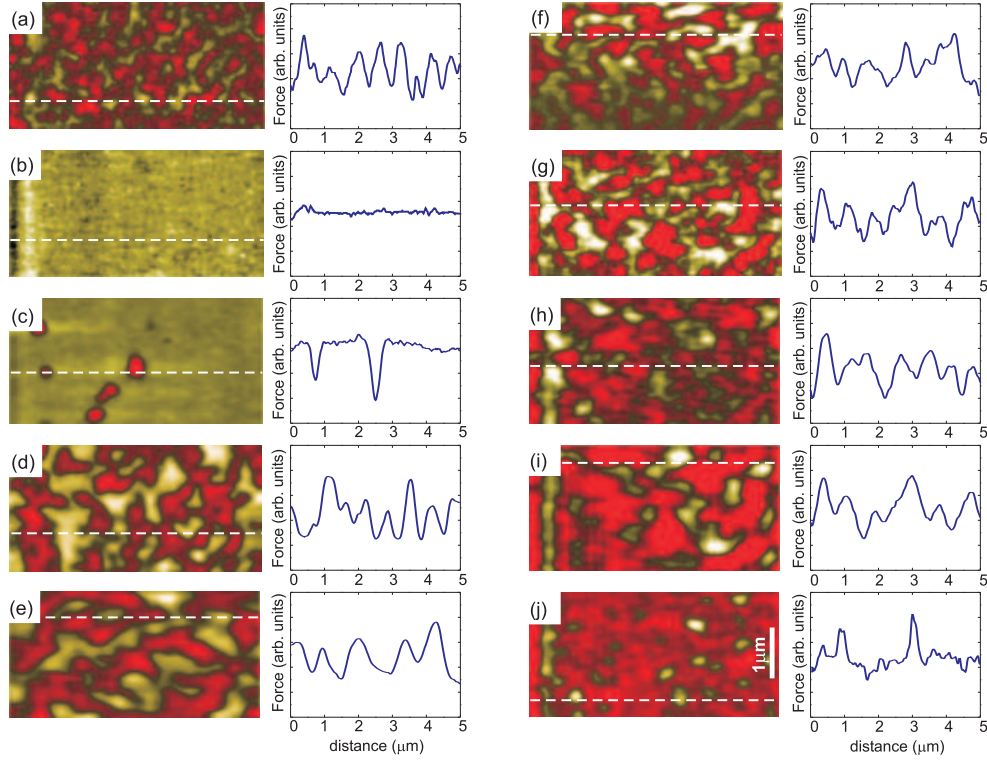


FIG. 5: (color online) Series of typical magnetic force microscopy (MFM) images for the sample $n=15$ measured at room temperature at $H = 0$ after applying of the magnetic field $H = H_{ret}$ perpendicular to the film plane. The images show the evolution of the magnetic domain structure over the same area $5 \times 2.5 \mu\text{m}^2$: (a) as-grown state, (b) positively magnetized state, (c) partially demagnetized state, $H_{ret} = -770 \text{ Oe}$, $|H_{ret}|/H_{c,15}^{300K} = 0.40$, (d) $H_{ret} = -1060 \text{ Oe}$, $|H_{ret}|/H_{c,15}^{300K} = 0.55$, (e) $H_{ret} = -1330 \text{ Oe}$, $|H_{ret}|/H_{c,15}^{300K} = 0.69$, (f) $H_{ret} = -1710 \text{ Oe}$, $|H_{ret}|/H_{c,15}^{300K} = 1.00$, (g) $H_{ret} = -1930 \text{ Oe}$, $|H_{ret}|/H_{c,15}^{300K} = 1.00$, (h) $H_{ret} = -2130 \text{ Oe}$, $|H_{ret}|/H_{c,15}^{300K} = 1.10$, (i) $H_{ret} = -2220 \text{ Oe}$, $|H_{ret}|/H_{c,15}^{300K} = 1.15$, (j) $H_{ret} = -2390 \text{ Oe}$, $|H_{ret}|/H_{c,15}^{300K} = 1.24$. The right-hand side panels of the images show normalized line traces of the measured magnetostatic forces taken across the dashed lines in the correspondent images.

larity of near-surface stray fields produced by ferromagnetic samples. This allows to obtain information about

the overall domain topology from an MFM image. A variable magnetic field module providing uniform fields

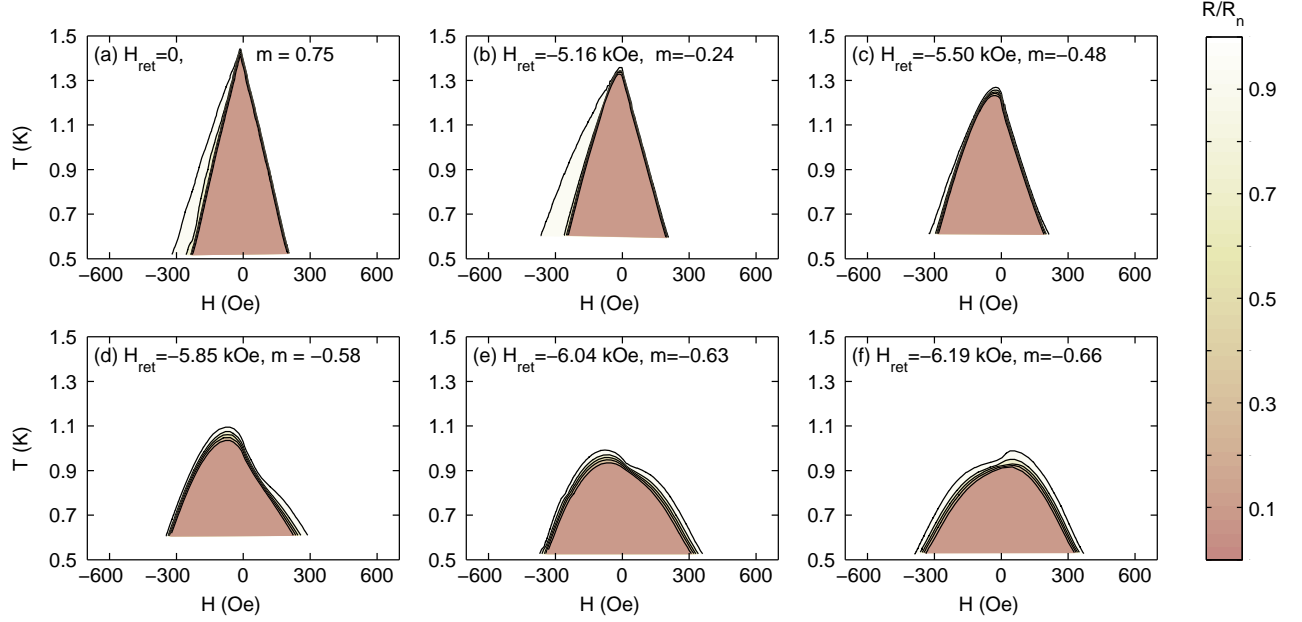


FIG. 6: (color online) Dc resistance of the sample n-10 as a function of H and T in different magnetic states. The returning H_{ret} fields and the normalized remanent magnetization $m = M_{ret}/M_{s,10}^{5K}$ are indicated on the plots. The darker shades correspond to lower resistance values. The solid lines are the level curves $R(H, T) = \alpha R_n$, where R_n is the resistance in normal state, $\alpha = 0.1, 0.3, 0.5, 0.7$ and 0.9 .

up to 4 kOe in the direction perpendicular to the sample surface was mounted on the MFM sample stage to study the evolution of the domain structure with varying H . The magnetic field module was used also to magnetize/demagnetize of the samples in-situ.

Figure 5 summarizes the evolution of the magnetic domains obtained for the sample n-15 for the different returning field values. We refer to this sample as the most representative. This figure shows the MFM images of the *same* area acquired at different magnetization states of the sample. In the first approximation, light and dark regions can be attributed to magnetic domains with different directions (signs) of the normal component of the local magnetic field, respectively. The right-hand side panels of the images show the normalized line traces of the measured magnetostatic forces taken across the the dashed lines in the correspondent images.

The panel (a) in Fig. 5 shows the domain pattern for the Co/Pt film in the as-grown state (before applying any magnetic field). Clearly, the length scales of the magnetic field variations appear to be smallest (the averaged width is about $0.3 \mu\text{m}$) and comparable with superconducting coherence length ($0.1 \mu\text{m}$ at $T = 0$, see estimates below). By magnetizing the sample, we remove all magnetic domains of the opposite direction with respect to the direction of the external magnetic field, and therefore there is no noticeable MFM contrast in the Fig. 5(b). Then, increasing the applied field, one gradually changes the shape and the size the magnetic domains of both polarities [panels (c)–(f) in Fig. 5]. The appearance of the

isolated negative domains in the positively magnetized matrix in the presence of the external magnetic field can be a plausible cause of the plateau on the descending branches of the $M(H)$ dependencies [see panels (a)–(c) in Fig. 2]. The size of the magnetic domains appears to be the smallest (but still larger than that in the as-grown state) at $|H| \simeq H_c$ [see Fig. 5 (g)]. Figure clearly portrays that the widths of positive and negative domains are rather close. This observation is consistent with the results presented in Fig. 4 which demonstrates that the remanent magnetization is close to zero. The final stage of the magnetization reversal is typical for ferromagnetic [Co/Pt] films: negative domains continue to grow and become dominant while the positive domains shrink in size [see Fig. 5 (h–j)]. The gradual increase of the area covered by the magnetized domains at increasing $|H_{ret}|$, what corresponds to the observed monotonous decrease of the magnetization, was confirmed by the performed analysis of the domain coverage.

III. TRANSPORT PROPERTIES OF S/F HYBRIDS

The measurements of the dc electrical resistance R as a function of temperature T and the external magnetic field H , applied perpendicularly to the plane of the S/F hybrid structures, were carried out in a commercial Oxford Instruments cryostat. The resistance was measured in the large-area specimens by a standard four-

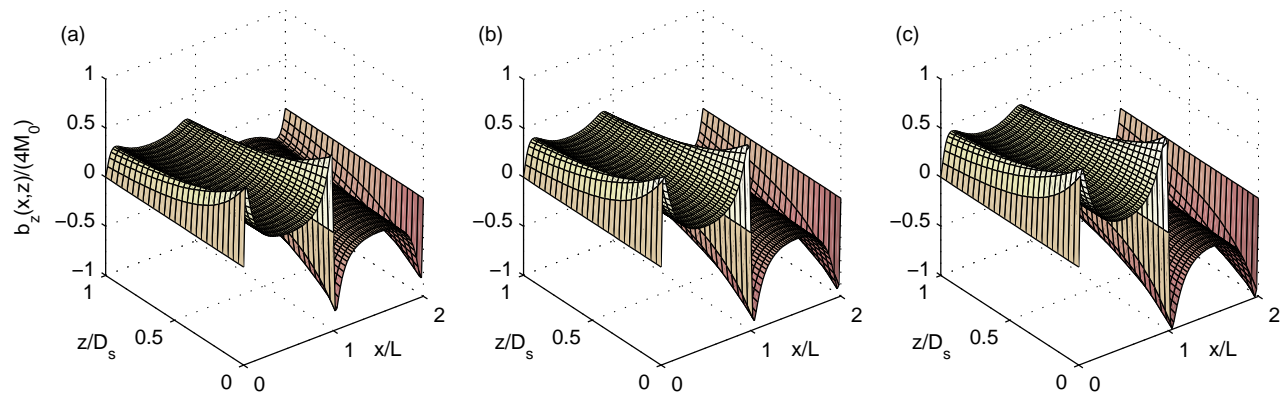


FIG. 7: (color online) The examples of the spatial distribution of the z -component of the magnetic field induced by one-dimensional periodic domain structure with out-of-plane magnetization inside the superconducting film for (a) $D_f = 16.5$ nm, (b) $D_f = 23.5$ nm, and (c) $D_f = 30.5$ nm. The regions $-D_f < z < 0$ and $0 < z < D_s$ correspond to the ferromagnetic and superconducting films, respectively. All other relevant parameters (D_s , equilibrium half-period L , the spacer h between the superconducting and ferromagnetic films, the magnetization M_0 etc.) are taken to be typical for our planar S/F structures, x -axis is taken perpendicular to the domain walls, see also Refs.^{16,18}

probe technique. The magnetic field produced by a superconducting magnet (up to 10^4 Oe) was used for a magnetization/demagnetization of the sample in-situ before the magnetoresistive measurements. The range of the H sweeping (from -700 Oe to 700 Oe) appears to be considerably smaller than the corresponding coercive fields of the ferromagnetic films at low temperatures (see Section II). Therefore we anticipate that the parameters of the domain structure, prepared by incomplete demagnetization, remains almost unaltered.

A. 10 bilayer sample

We begin with the discussion about the transport properties of the sample n-10 with the thinnest ferromagnetic [Co/Pt]₁₀ substrate.

For this sample which was preliminary magnetized in the positive direction we found out that the all level curves of the resistance $R(H, T) = \alpha R_n$ have the maxima positioned almost at $H = 0$, where R_n is the normal state resistance [panel (a) in Fig. 6]. It is worth noting that two level curves for $\alpha = 0.7$ and 0.9 are asymmetrical with respect to $H = 0$. In the other words, for a given temperature the resistance of the sample starts to deviate from its normal value at larger $|H|$ values for $H < 0$ than for $H > 0$. Currently we have no reliable interpretation of this asymmetry. A possible explanation is that the negative magnetic field $|H| > 50$ Oe induces the negatively magnetized domains, which disappear at the H inversion. However in our room temperature MFM measurements in the presence of the external magnetic field $H = -200$ Oe and $H = +200$ Oe we did not observe any change of the magnetic patterns and an appearance of such magnetic domains of the opposite polarity. We can attribute this to the restricted scan range and insufficient

sensitivity of our MFM microscope.

Nevertheless, the other level curves corresponding to low resistance criteria ($\alpha = 0.1, 0.3$ and 0.5) are almost symmetrical, and they practically coincide. It means that the conditions for a dropping of the resistance to zero are polarity-independent. Indeed, even if the isolated magnetic domains of opposite polarity appear reversibly at $H < 0$, they cannot ensure a vanishing of the electrical resistance. It is quite natural to attribute this lines to the upper critical field expression $H_{c2} = H_{c2}^{(0)}(1 - T/T_{c0})$, where the maximal critical temperature $T_{c0} = 1.45$ K and the upper critical field $H_{c2}^{(0)} = 368$ Oe at $T = 0$ were found from the optimal fitting. We would like to mention that the fitting gives us the same parameters T_{c0} and $H_{c2}^{(0)}$ for all three hybrid samples as we demonstrate below. This can be considered as an evidence of that the Al films have identical superconducting characteristics. Using the $H_{c2}^{(0)}$ value, we also estimated of the superconducting coherence length $\xi_0 = \sqrt{\Phi_0/(2\pi H_{c2}^{(0)})} = 93$ nm at $T = 0$.

During the procedure of the preparation of the magnetic state, one can irreversibly create negative magnetic domains by applying the external field H_{ret} of the order of the coercive field $H_{c,10}^{5K}$, as it follows from the MFM measurements at room temperature. The reduction of the averaged remanent magnetization results in the substantial suppression of the T_c maximum (up to 50%) [panels (b), (c) and (d) in Fig. 6]. The similar depletion of the maximal critical temperature was obtained for the same sample in as-grown state (not presented in this paper). At the same time the all maxima in the level curves $R(H, T) = \alpha R_n$ are shifted to negative H values of the order of 50–80 Oe depending on the H_{ret} values. This finding can be explained by a field compensation effect above the domains with positive mag-

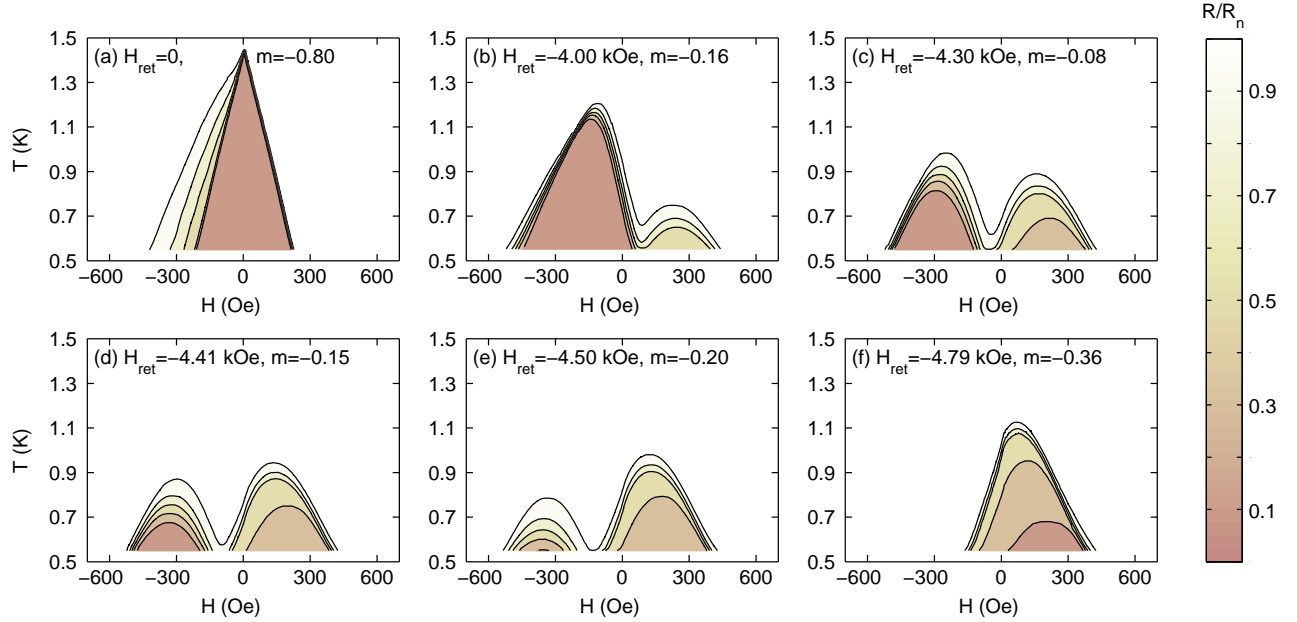


FIG. 8: (color online) Dc resistance of the sample n-15 as a function of H and T in different magnetic states. The returning H_{ret} fields and the normalized remanent magnetization $m = M_{ret}/M_{s,15}^{5K}$ are indicated on the plots. The darker shades correspond to lower dc resistance values. The solid lines are the level curves $R(H, T) = \alpha R_n$, where R_n is the resistance in normal state, $\alpha = 0.1, 0.3, 0.5, 0.7$, and 0.9 .

netization which are responsible for a percolation of the supercurrents at the initial stage of the magnetization reversal. Even a tiny change of the returning field essentially modifies the magnetoresistance of the hybrid structure: the maxima at the level curves which were initially positioned at $H < 0$, shift toward $H > 0$ and vice versa [panels (e)–(f) in Fig. 6]. In other words, we cannot observe the reentrant superconductivity for this sample for any H_{ret} parameter. In comparison with the samples n-15 and n-20 (see below) the displacement of the T_c maximum (~ 80 Oe) is too small. This indicates that both the amplitude and typical length scales of the built-in magnetic field are not large enough for a localizing of the order parameter in the compensated regions.

B. 15 bilayer sample

More interesting results were obtained for the sample with a 15 bilayer ferromagnetic film (the case of intermediate thickness of ferromagnetic substrate). One might conclude that an increase in the ferromagnetic film thickness will lead to

- (i) an increase of the typical width of the magnetic domains, since the equilibrium period of the domain structure with out-of-plane magnetization is proportional to $\sqrt{D_f}$, Ref.³⁶;
- (ii) an increase of the absolute value of the flux produced by the magnetic domains, since the smaller the D_f value, the faster the decay of the magnetic field in

the direction, perpendicular to the film plane, is;

- (iii) a decrease of the width of the magnetization curve, as it was revealed in the section II.

The first case (i) is difficult to verify in our experiments, since the parameters of the prepared domain structure are much more sensitive to the returning field values rather than to the thickness of the substrate. As far as the second case (ii) is concerned, we analyzed the spatial distribution of the z -component of the magnetic field induced by one-dimensional periodic domain structure, characterized by the period L and the magnetization M_s (Fig. 7). It is obvious that the increase in the thickness of ferromagnet raises the averaged field (or magnetic flux) emanating from the domains, since the magnetic field decays slower in the transverse direction as D_f increases (for a given domain's width).

The results of the transport measurements are summarized in Fig. 8. Analogous results obtained for the similar hybrid structure $\text{Al}(50 \text{ nm})/[\text{Co}/\text{Pt}]_{15}$ were partly presented in Refs.^{16,17}, in the form of a single curve of the constant resistance of the sample. However here we present complete information concerning the variations of magnetoresistance in full $T - H$ plane.

First of all we would like to note that the maximal critical temperature $T_{c0} = 1.45$ K of the sample n-15 in the fully magnetized state is the same as for the samples n-10 and n-20. In addition, all the level curves of the resistance for the uniformly magnetized sample are coincident straight lines (for the resistance ratios $\alpha = 0.1$ and

0.3) with the almost same slope $dT_c/dH \simeq T_{c0}/H_{c2}^{(0)}$ as for the samples n-10 and n-20. It clearly indicates that there are no differences in the superconducting properties of all hybrid samples.

The formation of isolated negative magnetic domains in the ferromagnetic film which is preliminary magnetized in a positive direction leads to a shift of the main T_c maximum toward negative H values and to a suppression of its amplitude [panel (b) in Fig. 8]. This can be easily explained by a compensation of the local magnetic field above rather wide positive magnetic domains. Such compensation leads to a preferred nucleation of superconductivity there¹⁶ (the regime of the reverse-domain superconductivity). At the same time the nucleation of superconductivity above negative magnetic domains, which have smaller typical width than positive domains (see Fig. 5) is energetically unfavorable. As a result, the T_c maximum at $H > 0$ has smaller amplitude. Indeed, as we argued in Refs.^{16,17}, the larger the area ℓ where the superconducting wave function is confined, the higher the critical temperature T_c of the appearance of such localized superconducting state is: $1 - T_c/T_{c0} \simeq \xi_0^2/\ell^2$. This effect can be interpreted as a quantum size effect for the localized superconducting wave function in non-uniform magnetic field, what is analogous to the standard quantum size effect for single electron wave function in a potential well.⁴ In addition, the maxima on all the level curves are also shifted, pointing out that superconductivity above positive domains is responsible for a percolation for supercurrents at lower temperatures.

A further increase of the H_{ret} value leading to a more pronounced decrease of the size of the positively magnetized domains, causes a suppression of the T_c maximum at $H < 0$ [panel (c) in Fig. 8]. This peak is now shifted to even higher negative fields, since the absolute value of the z -component of the stray field, (which has to be compensated), increases as the typical domain width decreases. Simultaneously, the growth of negatively magnetized domains results in a more favorable order parameter nucleation above negative domains and, accordingly, a second peak in the critical temperature at $H > 0$ becomes higher. Thus, two peaks corresponding to the reversed-domain superconductivity both above positive and negative domains are easily seen in the $H - T$ diagram. Taking the positions of these T_c maxima, once can estimate the amplitude of the nonuniform magnetic field, which is of the order of 300 Oe. In the vicinity of the coercive field even small H_{ret} variation can induce a evident change in the relative amplitude of the T_c peaks, which should be attributed to the reshuffling or reshaping of the magnetic domains [compare panels (c) and (d) in Fig. 8]. We would like to note that the level curves for high and low resistance ratio (e.g. $\alpha = 0.1$ and 0.9) may have completely different shapes. For instance, the nucleation of superconductivity (i.e. an initial decrease of the resistance) can occur both at the positive and negative compensation fields almost at the same temperature, however the sample's resistance goes to zero only

at $H < 0$ [panel (d) in Fig. 8]. We interpret this finding as a consequence of the effect of current percolation in a irregular labyrinth-type domain pattern.

Interestingly, the shape of the level curve for $\alpha = 0.9$ quite well resembles the non-monotonous dependence $T_c(H)$ with positive curvature at small H values, predicted theoretically for the regime of the domain-wall superconductivity.¹¹⁻¹³ We would like to interpret our result as a fingerprint of the possible crossover between reverse-domain superconductivity and domain-wall superconductivity at sweeping H [panels (c)–(e) in Fig. 8].

For higher H_{ret} values the first peak, located at negative fields, disappears, whereas the peak at positive fields shifts up in temperature and is displaced to a lower field curve [panels (e)–(f) in Fig. 8]. This second peak will eventually evolve into a linear phase boundary when the ferromagnetic film becomes fully magnetized in the negative direction.

C. 20 bilayer sample

Finally, we briefly discuss the superconducting properties of the sample n-20 with the thickest ferromagnetic substrate. The general evolution of the magnetoresistance at varying H_{ret} parameter is quite similar to that for the sample n-15 (compare Figs. 8 and 9). For the sample in the demagnetized state ($|H_{ret}| \sim H_c$) the effect of the stray field of the magnetic domains is so strong that we can observe only the initial stage of the decrease of the electrical resistance at the compensation fields in very narrow range of available temperatures [panels (d) and (e) in Fig. 9]. This displacement of the T_c maxima to the higher H values (400–500 Oe) as well as the lowering of the critical temperature at $H = 0$ are in agreement with our explanation concerning the increase of the averaged magnetic field produced by the magnetic domains in thick ferromagnetic films.

Currently we cannot explain the observed global suppression of the maximal critical temperature near the compensation fields [panels (d) and (e)]. For instance, this effect can be caused by considerable shrinkage of the domain width down to the length scales comparable with ξ_0 . However, typical width of magnetic domains for sample n-20 does not differ considerably from that for the sample n-15 as it follows from the MFM measurements. Therefore we might expect the essential modification of the remanent distribution of magnetization for thick ferromagnetic film, e.g. an increase in the in-plane component of the magnetic moments. Anyway, the clarification of the origin of the global suppression of superconductivity in the S/F hybrids with thick multilayered ferromagnetic films deserves a separate detailed study.

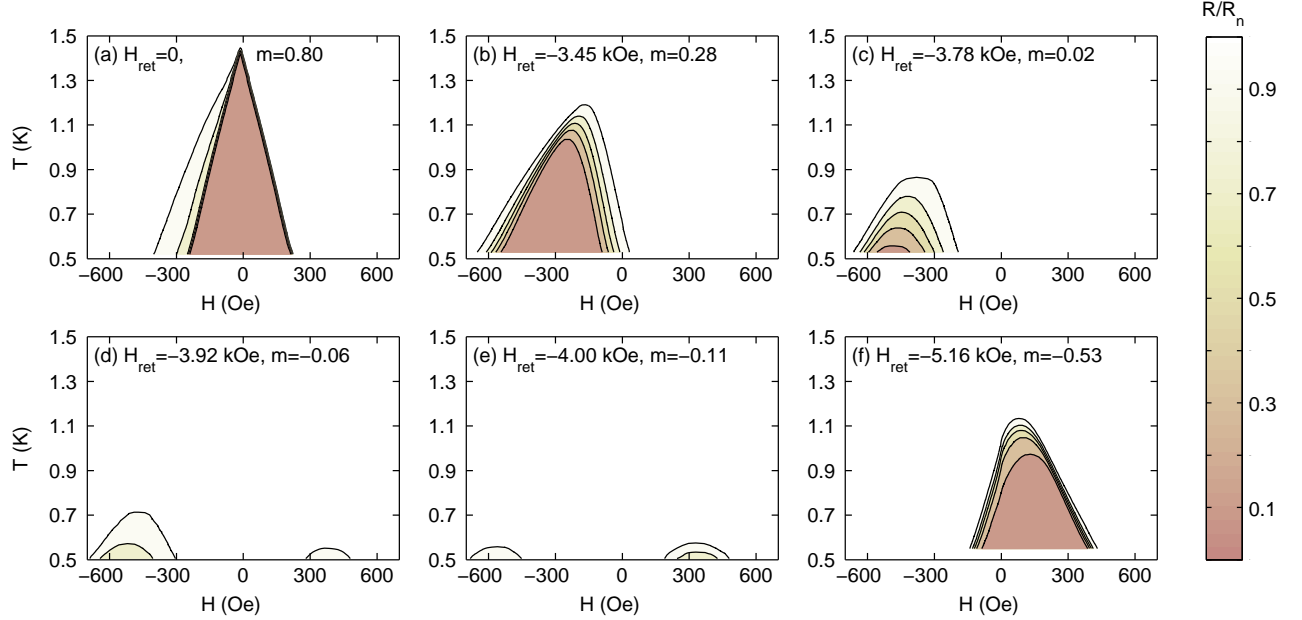


FIG. 9: (color online) Dc resistance of the sample n=20 as a function of H and T in different magnetic states. The returning H_{ret} fields and the normalized remanent magnetization $m = M_{ret}/M_{s,20}^{5K}$ are indicated on the plots. The darker shades correspond to lower dc resistance values. The solid lines are the level curves $R(H, T) = \alpha R_n$, where R_n is the resistance in normal state, $\alpha = 0.1, 0.3, 0.5, 0.7$, and 0.9 .

IV. CONCLUSION

We investigated experimentally the peculiarities of the electrical transport on large-area superconducting aluminum films deposited on top of multilayered ferromagnetic $[\text{Co/Pt}]_n$ structure (n is the number of the bilayers). We demonstrated that: (i) by changing the n value during the fabrication process and (ii) by varying the remanent magnetization of the hybrid sample during the demagnetization procedure, one can control a spatial distribution of the magnetic field, induced by magnetic domains, inside the superconducting film. We showed that the nonuniform magnetic field generated by magnetic bubble domains strongly modifies the dependence of the electrical resistance of the sample on temperature T and the external magnetic field H . We found out that the behavior of the planar S/F hybrids at temperatures close to the critical temperature of the superconducting transition and at low temperatures can be completely different: the nucleation of superconductivity is governed mainly by the typical lateral dimensions of the magnetic domains regardless their shapes, while at low temperatures the general topology of the magnetic pattern becomes very important.

We demonstrated that the increase in the ferromagnetic film thickness leads to the more pronounced reentrant superconductivity, characterized by a decrease of the resistance as H increases. However further increase of the n number suppresses the critical temperature of

the hybrid sample. Thus for the planar Al-based hybrid structures we determined an optimal thickness of the ferromagnetic film ($n = 15$), when the non-monotonous dependence of the superconducting critical temperature on H can be observed in rather wide T and H range. This finding can be of interest, e.g., for further experimental investigations of the different regimes of the localized superconductivity in the presence of magnetic templates. Indeed, the observed parabolic dependence $T_c = \alpha_0 + \alpha_1 |H|^2$ can indicate the superconductivity localized near magnetic domain walls (α_0, α_1 are positive constants). Nevertheless the problem concerning the direct visualization of the domain-wall superconductivity in the S/F hybrids is still challenging. The formation of the localized superconductivity (both the domain-wall superconductivity and the reverse-domain superconductivity) can be detected by means of the scanning tunnelling microscopy/spectroscopy (STM/STS). However a matching between the magnetic pattern and the distribution of the local density of states can be performed in a case of domain structure with unalterable small-scale domain structure. In addition, rather high amplitude of the magnetic field is necessary to guarantee the localization of the superconducting wave function near the domain walls. Thus, the parameters of the domain structure in the multilayered $[\text{Co/Pt}]_n$ films meet these requirements. Therefore the planar S/F hybrids with the optimal composition, resulting in the well-defined reentrant superconductivity, can be effectively used for the high-resolution STM/STS investigations of the systems revealing the lo-

calized superconductivity.

We thank W. Gillijns and B. Opperdoes for technical support and D. Rodichev for valuable comments. This work was supported by the Methusalem Funding of the Flemish Government, the NES – ESF program, the Belgian IAP, the Fund for Scientific Research – Flanders

(F.W.O.–Vlaanderen), the Russian Fund for Basic Research, RAS under the Program “Quantum physics of condensed matter”, Russian Agency of Education under the Federal Program “Scientific and educational personnel of innovative Russia in 2009–2013” and the Presidential grant MK-4880.2008.2.

-
- * Electronic address: aladyshkin@ipm.sci-nnov.ru
- ¹ J.I. Martín, J. Nogués, K. Liu, J.L. Vicente and I.K. Schuller, *J. Magn. Magn. Mater.* **256**, 449 (2003).
 - ² I.F. Lyuksyutov and V.L. Pokrovsky, *Adv. Phys.* **54**, 67 (2005).
 - ³ M. Vélez, J.I. Martín, J.E. Villegas, A. Hoffmann, E.M. Gonzalez, J.L. Vicent and I.K. Schuller, *J. Magn. Magn. Mater.* **320**, 2547 (2008).
 - ⁴ A.Yu. Aladyshkin, A.V. Silhanek, W. Gillijns, and V.V. Moshchalkov, *Supercond. Sci. Tech.* **22**, 053001 (2009).
 - ⁵ L.N. Bulaevskii, A.I. Buzdin, M.L. Kulić and S.V. Panyukov, *Adv. Phys.* **34**, 175 (1985).
 - ⁶ Yu.A. Izyumov, M.G. Khusainov and Yu.N. Proshin, *Phys.-Usp.* **45**, 109 (2002).
 - ⁷ A.I. Buzdin, *Rev. Mod. Phys.* **77**, 935 (2005).
 - ⁸ F.S. Bergeret, A.F. Volkov and K.B. Efetov, *Rev. Mod. Phys.* **77**, 1321 (2005).
 - ⁹ Y. Otani, B. Pannetier, J.P. Nozières and D. Givord, *J. Magn. Magn. Mater.* **126**, 622 (1993).
 - ¹⁰ A.Yu. Aladyshkin, A.S. Mel’nikov, D.A. Ryzhov, *J. Phys.: Condens. Matter* **15**, 6591 (2003).
 - ¹¹ A.I. Buzdin and A.S. Mel’nikov, *Phys. Rev. B* **67**, 020503 (R) (2003).
 - ¹² A.Yu. Aladyshkin, A.I. Buzdin, A.A. Fraerman, A.S. Mel’nikov, D.A. Ryzhov, and A.V. Sokolov, *Phys. Rev. B* **68**, 184508 (2003).
 - ¹³ A.Yu. Aladyshkin and V.V. Moshchalkov, *Phys. Rev. B* **74**, 064503 (2006).
 - ¹⁴ M. Lange, M.J. Van Bael, Y. Bruynseraede, and V.V. Moshchalkov, *Phys. Rev. Lett.* **90**, 197006 (2003).
 - ¹⁵ W. Gillijns, A.V. Silhanek and V.V. Moshchalkov, *Phys. Rev. B* **74**, 220509(R) (2006).
 - ¹⁶ W. Gillijns, A.Yu. Aladyshkin, A.V. Silhanek, and V.V. Moshchalkov, *Phys. Rev. B* **76**, 060503 (R) (2007).
 - ¹⁷ A.Yu. Aladyshkin, W. Gillijns, A.V. Silhanek, V.V. Moshchalkov, *Physica C* **468**, 737 (2008).
 - ¹⁸ W. Gillijns, A.Yu. Aladyshkin, M. Lange, M.J. Van Bael, V.V. Moshchalkov, *Phys. Rev. Lett.* **95**, 227003 (2005).
 - ¹⁹ Z. Yang, M. Lange, A. Volodin, R. Szymczak and V.V. Moshchalkov, *Nature Materials* **3**, 793 (2004).
 - ²⁰ Z. Yang, K. Vervaeke, V.V. Moshchalkov, R. Szymczak, *Phys. Rev. B* **73**, 224509 (2006).
 - ²¹ Z. Yang, J. Van de Vondel, W. Gillijns, W. Vinckx, and V.V. Moshchalkov, *Appl. Phys. Lett.* **88**, 232505 (2006).
 - ²² J. Fritzsche, V.V. Moshchalkov, H. Eitel, D. Koelle, R. Kleiner, and R. Szymczak, *Phys. Rev. Lett.* **96**, 247003 (2006).
 - ²³ A.Yu. Aladyshkin, J. Fritzsche, and V.V. Moshchalkov, *Appl. Phys. Lett.* **94**, 222503 (2009).
 - ²⁴ J. Fritzsche, R.B.G. Kramer, and V.V. Moshchalkov, *Phys. Rev. B* **80**, 094514 (2009).
 - ²⁵ A.Yu. Aladyshkin, J. Fritzsche, and V.V. Moshchalkov, *Physica C*, submitted (2009).
 - ²⁶ L.Y. Zhu, T.Y. Chen, and C.L. Chien, *Phys. Rev. Lett.* **101**, 017004 (2008).
 - ²⁷ R.K. Rakshit, R.C. Budhani, T. Bhuvana, V.N. Kulkarni, and G.U. Kulkarni, *Phys. Rev. B* **77**, 052509 (2008).
 - ²⁸ R.K. Rakshit, S.K. Bose, R. Sharma, N.K. Pandey, and R.C. Budhani, *Phys. Rev. B* **77**, 094505 (2008).
 - ²⁹ C. Bell, S. Tursucu, and J. Aarts, *Phys. Rev. B* **74**, 214520 (2006).
 - ³⁰ V.K. Vlasko-Vlasov, U. Welp, A. Imre, D. Rosenmann, J. Pearson, and W. K. Kwok, *Phys. Rev. B* **78**, 214511 (2008).
 - ³¹ V. Vlasko-Vlasov, U. Welp, G. Karapetrov, V. Novosad, D. Rosenmann, M. Iavarone, A. Belkin, and W.-K. Kwok, *Phys. Rev. B* **77**, 134518 (2008).
 - ³² A. Belkin, V. Novosad, M. Iavarone, J. Fedor, J. E. Pearson, A. Petrean-Troncalli, and G. Karapetrov, *Appl. Phys. Lett.* **93**, 072510 (2008).
 - ³³ A. Belkin, V. Novosad, M. Iavarone, J. Pearson, and G. Karapetrov, *Phys. Rev. B* **77**, 180506 (2008).
 - ³⁴ W.B. Zeper, F.J.A.M. Greidanus, P.F. Carcia and C.R. Fincher, *J. Appl. Phys.* **65**, 4971 (1989).
 - ³⁵ M. Lange, M.J. Van Bael, V.V. Moshchalkov, and Y. Bruynseraede, *Appl. Phys. Lett.* **81**, 322 (2002).
 - ³⁶ L.D. Landau and E.M. Lifshitz, *Electrodynamics of Continuous Media*, Second Edition: Volume 8 (Course of Theoretical Physics) (Pergamon Press, 1984).